Nitrosomonas europaea cytochrome P460 is a direct link between nitrification and nitrous oxide emission

Jonathan D. Caranto[a,1], Avery C. Vilbert[a,1], and Kyle M. Lancaster[a,2]

[a]Department of Chemistry and Chemical Biology, Baker Laboratory, Cornell University, Ithaca, NY 14853

Edited by Stephen J. Lippard, Massachusetts Institute of Technology, Cambridge, MA, and approved October 20, 2016 (received for review July 6, 2016)

Ammonia oxidizing bacteria (AOB) are major contributors to the emission of nitrous oxide (N_2O). It has been proposed that N_2O is produced by reduction of NO. Here, we report that the enzyme cytochrome (cyt) P460 from the AOB *Nitrosomonas europaea* converts hydroxylamine (NH_2OH) quantitatively to N_2O under anaerobic conditions. Previous literature reported that this enzyme oxidizes NH_2OH to nitrite (NO_2^-) under aerobic conditions. Although we observe NO_2^- formation under aerobic conditions, its concentration is not stoichiometric with the NH_2OH concentration. By contrast, under anaerobic conditions, the enzyme uses 4 oxidizing equivalents (eq) to convert 2 eq of NH_2OH to N_2O. Enzyme kinetics coupled to UV/visible absorption and electron paramagnetic resonance (EPR) spectroscopies support a mechanism in which an Fe^{III}–NH_2OH adduct of cyt P460 is oxidized to an $\{FeNO\}^6$ unit. This species subsequently undergoes nucleophilic attack by a second equivalent of NH_2OH, forming the N–N bond of N_2O during a bimolecular, rate-determining step. We propose that NO_2^- results when nitric oxide (NO) dissociates from the $\{FeNO\}^6$ intermediate and reacts with dioxygen. Thus, NO_2^- is not a direct product of cyt P460 activity. We hypothesize that the cyt P460 oxidation of NH_2OH contributes to NO and N_2O emissions from nitrifying microorganisms.

nitric oxide | nitrification | nitrous oxide | enzymology | bioinorganic chemistry

Nitrous oxide (N_2O) participates in ozone-layer depletion and possesses a global warming potential nearly 300-fold greater than carbon dioxide (1). Atmospheric N_2O concentrations have increased ∼120% since the preindustrial era, largely due to the widespread use of fertilizers required to produce sustenance for humans and livestock. N_2O is a byproduct of the microbial metabolism of fertilizer components, including ammonia (NH_3) and nitrate (NO_3^-); consequently, agricultural soils account for an estimated 60–75% of global N_2O emissions. The metabolic pathway by which microorganisms oxidize NH_3, nitrification, occurs in two phases, both of which are mediated by autotrophic microorganisms. In the first, NH_3-oxidizing bacteria (AOB) or archaea (AOA) oxidize NH_3 to nitrite (NO_2^-). In the second, NO_2^- is subsequently oxidized to NO_3^- by NO_2^--oxidizing bacteria. NH_3-oxidizing microbes contribute substantially to global N_2O emissions, whereas NO_2^--oxidizing bacteria produce negligible N_2O (2, 3). AOB are proposed to emit N_2O either as a byproduct of the nitrification pathway or as a product of the nitrifier denitrification pathway (i.e., the reduction of NO_2^-) (4–6).

Nitrification of NH_3 to NO_2^- occurs in two steps (7, 8). The first step is catalyzed by NH_3 monooxygenase, which uses copper (Cu) and dioxygen (O_2) to hydroxylate NH_3 to hydroxylamine (NH_2OH) (9). In AOB, the second step is thought to be the four-electron oxidation of NH_2OH to NO_2^- by NH_2OH oxidoreductase (HAO). HAO is a multiheme enzyme with eight *c*-type hemes per subunit: seven are electron transfer cofactors, and the eighth is the so-called P460 active site that contains a unique tyrosine cross-link to the heme ring. The enzyme (or enzymes) that AOA uses to oxidize NH_2OH is currently unknown (10).

AOB possess machinery for nitrifier denitrification that reduces NO_2^- to N_2O via a nitric oxide (NO) intermediate (11, 12). The archetypal AOB *Nitrosomonas europaea* possesses genes for a Cu-containing nitrite reductase (NirK) and a membrane-bound, heme-containing NO reductase (NorB). NirK reduces NO_2^- by one electron to NO, whereas NorB catalyzes the two-electron reduction of 2 eq of NO to N_2O. Nitrifier denitrification is thought to lead to the increased production of N_2O and NO by AOB in microaerophilic or anaerobic conditions (13). However, this pathway does not account for the total AOB N_2O emission under aerobic conditions.

Under aerobic conditions, N_2O emission from AOB is proposed to result from the incomplete oxidation of NH_2OH to either nitroxyl (HNO) or NO. Two eq of HNO rapidly react to form N_2O (14), whereas NO is reduced by an NO reductase (12). In support of these hypotheses, both NO and N_2O have been observed to form during steady-state turnover of purified HAO under aerobic conditions (15). Although NorB could facilitate this N_2O production, a NorB knockout strain also produces N_2O at atmospheric O_2 concentration, consistent with the presence of an alternate N_2O-producing pathway (16).

In this study, we demonstrate that there indeed exists a direct enzymatic pathway from NH_2OH to N_2O, and that this pathway is mediated by cytochrome (cyt) P460, a constitutively expressed (17), soluble, periplasmic metalloenzyme originally isolated from *N. europaea* (18). *N. europaea* cyt P460 is a 36-kDa homodimeric protein in which each subunit bears a mono-His *c*-type heme with an N–C cross-link from the 13′ mesocarbon to the amine of Lys70 (19) (Fig. 1*A*). Such cross-links alter porphyrin π-conjugation. Moreover, the heme P460 macrocycle exhibits significant ruffling, a common distortion mode for *c*-type hemes (20, 21). P460 hemes are named for the 460-nm Soret band observed in their ferrous state. The P460 center found in *N. europaea* HAO differs from cyt P460: it is doubly cross-linked by Tyr491 at the 5′ mesocarbon and an adjacent pyrrole α-carbon (Fig. 1*B*). Despite lacking homology to HAO (19, 22), the presence of a P460 cofactor in cyt P460 has implicated this enzyme in NH_2OH oxidation (23–25).

Significance

Nitrous oxide (N_2O) is a potent ozone-depleting greenhouse gas. This work identifies a means by which N_2O is generated during nitrification, or biological ammonia oxidation. Fertilizer use in agriculture stimulates nitrification, thus increasing the volume of N_2O emissions worldwide. The results presented herein will inform models and strategies toward optimized, sustainable agriculture. Moreover, these results highlight a rare example of biological N–N bond formation.

Author contributions: K.M.L. designed research; J.D.C. and A.C.V. performed research; J.D.C., A.C.V., and K.M.L. analyzed data; and J.D.C., A.C.V., and K.M.L. wrote the paper.

The authors declare no conflict of interest.

This article is a PNAS Direct Submission.

See Commentary on page 14474.

[1]J.D.C. and A.C.V. contributed equally to this study.

[2]To whom correspondence should be addressed. Email: kml236@cornell.edu.

This article contains supporting information online at www.pnas.org/lookup/suppl/doi:10.1073/pnas.1611051113/-/DCSupplemental.

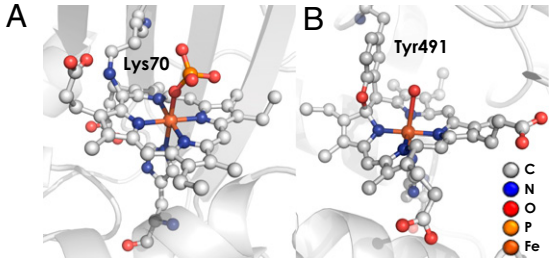

Fig. 1. Ferric P460 cofactors in cyt P460 [*A*, Protein Data Bank (PDB) ID code 2JE2] and HAO (*B*, PDB ID code 4N4N).

Cyt P460 was previously reported to oxidize NH_2OH to NO_2^- (26), implicating all P460 centers in mediating four-electron oxidation of NH_2OH. However, an octaheme HAO-like protein from the anaerobic NH_3-oxidizing microorganism *Kuenenia stuttgartiensis* was shown to oxidize NH_2OH to NO instead of NO_2^- (27). An X-ray crystal structure of the *K. stuttgartiensis* HAO-like enzyme features a tyrosine cross-linked active site and heme distribution that was identical to *N. europaea* HAO. The *K. stuttgartiensis* enzyme was proposed to yield NO due to the absence of a nearby tyrosine residue that is present in *N. europaea* HAO. The *N. europaea* cyt P460 active site also lacks the nearby tyrosine residue and is far more solvent-exposed (19). Herein, we show that N_2O is the enzymatic product of anaerobic NH_2OH oxidation by *N. europaea* cyt P460. We demonstrate that this pathway proceeds through an NH_2OH-bound form that is oxidized by three electrons to an Fe–NO species that then reacts with NH_2OH to form N_2O in the rate-determining step.

Results and Discussion

Exclusive Conversion of NH_2OH to N_2O by Cyt P460 Under Anaerobic Conditions. Consistent with previous work on the *Methylococcus capsulatus* cyt P460 (26), under aerobic conditions, cyt P460 reacts with NH_2OH in the presence of the oxidant phenazine methosulfate (PMS) to form NO_2^-, as detected by Griess diazotization assays (*SI Appendix*, Fig. S1*A*). However, the maximum stoichiometry achieved was 0.7 mol of NO_2^- per mole of NH_2OH (*SI Appendix*, Table ST1). Gas chromatography (GC) analysis reveals that the remainder of the NH_2OH is converted to N_2O (*SI Appendix*, Fig. S1*A*).

Under anaerobic conditions, no NO_2^- is formed when cyt P460 is treated with NH_2OH and PMS. GC analysis (*SI Appendix*, Fig. S1*B*) reveals that in the presence of an oxidant ($[Ru(NH_3)_6]Cl_3$, horse heart cyt *c*, or PMS), cyt P460 catalyzes the exclusive formation of N_2O from NH_2OH. In the absence of either enzyme or oxidant, only trace N_2O is formed (*SI Appendix*, Fig. S1). By monitoring the amount of N_2O produced under various NH_2OH or oxidant concentrations (Fig. 2*A*), a stoichiometry of 2 NH_2OH eq and 4 oxidizing eq producing 1 eq of N_2O was established (Eq. **1**):

$$2\ NH_2OH \rightarrow N_2O + H_2O + 4\ e^- + 4\ H^+. \qquad [1]$$

Steady-State Kinetics. Steady-state activity assays of cyt P460 were performed under anaerobic conditions using a 2,6-dichlorophenolindophenol (DCPIP)/PMS coupled assay (23) and an N_2O-selective electrode. By monitoring the decay of the DCPIP absorbance at 605 nm (A_{605}), it was determined that 2 eq of DCPIP was reduced per 1 eq of N_2O produced under steady-state conditions (*SI Appendix*, Fig. S2). Because DCPIP is a two-electron oxidant, this stoichiometry is consistent with Eq. **1**. The DCPIP/PMS assay therefore provides a convenient means of measuring steady-state N_2O production by cyt P460.

Steady-state activities of cyt P460 have been reported previously (23, 26), but to our knowledge, no studies have presented steady-state activity plots. Fig. 2*B* shows the steady-state activity plot exhibiting nonsaturating, linear behavior from 0.05 to 20 mM NH_2OH that spans turnover frequencies of 0.3–80 μM DCPIP consumed $min^{-1}{\cdot}\mu M{\cdot}enzyme^{-1}$. Although this nonsaturating behavior precludes determination of k_{cat} or K_m, the slope of the linear region suggests a k_{cat}/K_m of 5,000 $M^{-1}{\cdot}min^{-1}$ (28). However, the characterization of pathway intermediates suggests a multistep reaction mechanism that is inconsistent with classical Michaelis–Menten kinetics (*vide infra*).

Characterization of Cyt P460 Fe^{III}–NH_2OH. Recombinant expression and purification of cyt P460 was previously achieved by Elmore et al. (29). This method yields a British racing green protein with UV/visible absorption and electron paramagnetic resonance (EPR) spectra consistent with those reported for the enzyme isolated from *N. europaea* (18, 23, 30). The absorption spectrum of the as-isolated cyt P460 has a Soret band at 440 nm with a shoulder at 414 nm and Q-band maxima at 570 nm and 627 nm (Fig. 3). The corresponding EPR spectrum (Fig. 4*A*) is characteristic of an $S = {}^5/_2$ Fe^{III}, with *g*-values of 6.57, 5.09, and 1.97 ($^E/_D = 0.03$). The crystal structure of the as-isolated cyt P460 (19, 29) (Fig. 1*A*) shows phosphate ligated to the Fe center. These crystallization conditions used 2.4 M phosphate buffer; we expect that H_2O will occupy this site under our experimental conditions, and therefore assign the as-isolated protein as an Fe^{III}–OH_2 heme center.

The addition of NH_2OH to cyt P460 produces a species with a UV/visible absorption spectrum distinct from Fe^{III}–OH_2 (Fig. 3). Within the time of manual mixing, the 414-nm shoulder of the Fe^{III}–OH_2 spectrum disappears concomitant with a shift in the Soret band to 445 nm and broadening of the Q-bands. The simplest interpretation is that NH_2OH substitutes for H_2O at the Fe site (i.e., Fe^{III}–NH_2OH). Cyt P460 was titrated with NH_2OH, and the resulting series of spectra (*SI Appendix*, Fig. S3*A*) show an isosbestic point at 438 nm, which suggests a one-step conversion from Fe^{III}–OH_2 to the putative Fe^{III}–NH_2OH. To determine the NH_2OH dissociation constant [$K_{d(NH_2OH)}$], the absorption at 414 nm (A_{414}) was plotted against NH_2OH concentration. Fitting the data to a hyperbolic binding curve resulted in a $K_{d(NH_2OH)}$ of 9 ± 1 mM (*SI Appendix*, Fig. S3*A*, *Inset*).

Treatment of cyt P460 with 100 mM NH_2OH results in the disappearance of the $S = {}^5/_2$ Fe^{III}–OH_2 signal and the appearance of two rhombic $S = {}^1/_2$ EPR signals (Fig. 4*B*). The first

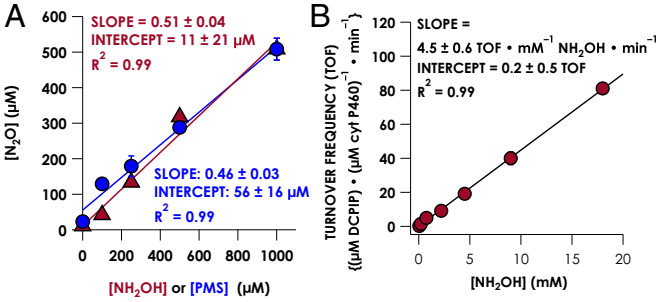

Fig. 2. (*A*) Stoichiometry of N_2O production by cyt P460 determined with GC. Data points are averages of triplicate trials with 5 μM ferric cyt P460 in anaerobic 50 mM Hepes, pH 8.0, at 25 °C overnight. Error bars represent 1 SD of three trials. For the red triangles, the concentration of PMS is held at 1 mM, whereas the NH_2OH concentration is varied; for the blue circles, the NH_2OH concentration is held at 1 mM, whereas PMS concentration varies. (*B*) Steady-state NH_2OH oxidase activity plot for cyt P460. The assay conditions were 1 μM cyt P460, 6 μM PMS, and 100 μM DCPIP with various NH_2OH concentrations in anaerobic 50 mM Hepes, pH 8.0, at 25 °C. Each data point is the average of three trials, with error bars representing one SD.

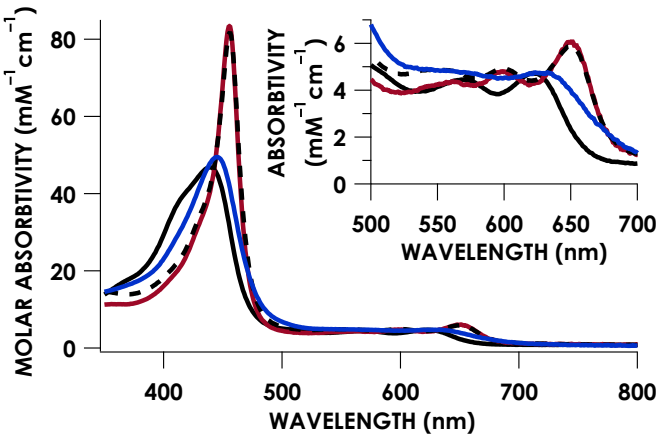

Fig. 3. UV/visible absorption spectra of Fe^{III}–OH_2 cyt P460 (black), Fe^{III}–NH_2OH cyt P460 (blue), and $\{FeNO\}^6$ cyt P460 generated via treatment with PROLI-NONOate (red line) or oxidation of Fe^{III}–NH_2OH (black dashed line). (*Inset*) Magnification of the Q-bands.

signal has *g*-values of 2.75, 2.28, and 1.54, and is consistent with a low-spin Fe^{III}. The EPR spectra of cyt P460 treated with increasing concentrations of NH_2OH (*SI Appendix*, Fig. S3*B*) corroborate the $K_{d(NH_2OH)}$ value determined with UV-vis spectrometry. The conversion from a high-spin to low-spin Fe^{III} is consistent with the binding of NH_2OH to the Fe center; thus, we assign this $S = {}^1/_2$ species as a rare example of a stable heme Fe^{III}–NH_2OH complex (31).

The second rhombic $S = {}^1/_2$ signal has *g*-values of 2.10, 2.02, and 2.01, and ^{14}N hyperfine coupling values of 50 MHz, 57 MHz, and 45 MHz. This second signal represents less than 5% of the total spin as determined by spin quantitation and is consistent with a five-coordinate heme Fe^{II}–NO species (32), or $\{FeNO\}^7$ in Enemark–Feltham notation (33). This $\{FeNO\}^7$ species can be independently generated by treating cyt P460 with the HNO donor, disodium diazen-1-ium-1,2,2 triolate ($Na_2N_2O_3$, Angeli's salt). This species is stable in the presence of NH_2OH or oxidant (*SI Appendix*, Fig. S4). The low yield observed in the EPR spectrum and the lack of reactivity suggest that the $\{FeNO\}^7$ is an off-path product and does not contribute to the productive N_2O-generating cyt P460 pathway. At present, we are unsure why this oxidized species appears in the absence of O_2, oxidant, or NO. One possibility is that the samples are exposed to a small amount of O_2 during freezing, which would oxidize Fe^{III}–NH_2OH to $\{FeNO\}^7$.

Characterization of an Intermediate in NH_2OH Oxidation. The addition of the oxidant $[Ru(NH_3)_6]Cl_3$ under anaerobic conditions results in formation of a new species. Over the course of the reaction (*ca.* 20 min), there are two distinct phases: an accumulation phase and a decay phase. In the accumulation phase, a new species appears within 2 min. The absorption spectrum of the new species exhibits an intense and sharp Soret band centered at 455 nm and Q-bands at 554 nm, 603 nm, and 652 nm (*SI Appendix*, Fig. S5*A*). Several isosbestic points are observed during the spectral time course, indicating a single-step conversion from Fe^{III}–NH_2OH to the new species. In the decay phase, the new species is converted back to Fe^{III}–NH_2OH. The spectral time course of this phase also features several isosbestic points (*SI Appendix*, Fig. S5*B*). These data strongly suggest the accumulation and decay of an intermediate on the cyt P460 pathway, hereafter referred to as the 455-nm intermediate owing to its Soret band maximum.

In the presence of DCPIP, the formation of the 455-nm intermediate is complete at the time of mixing; the intermediate persists for 1 min, until DCPIP is completely consumed, at which point the A_{455} slowly decreases (*SI Appendix*, Fig. S6). Subsequent addition of 10 mM NH_2OH hastened the decay of the 455-nm intermediate (*SI Appendix*, Fig. S6*C*). The spectral time course of the decay phase features an isosbestic point at 445 nm, consistent with the direct conversion of the 455-nm intermediate to a single species. Comparison of the final decay product spectrum to the decay product of as-isolated cyt P460 mixed with 10 mM NH_2OH confirms that the decay product is Fe^{III}–NH_2OH (*SI Appendix*, Fig. S6*B*).

The persistence of the 455-nm intermediate in the presence of excess oxidant suggests that, under turnover conditions, the decay of the 455-nm intermediate is the rate-determining step. The increase in decay rate at higher NH_2OH concentrations implies a bimolecular reaction between the 455-nm intermediate and NH_2OH. To confirm this relationship, the formation and decay of the 455-nm intermediate at various NH_2OH concentrations were monitored (*SI Appendix*, Fig. S8*A*). The sum of two exponentials (*SI Appendix*, Eq. **S1**) was fit to the A_{455} traces, providing observed rate constants (k_{obs}) for both the formation [$k_{obs(1)}$] and decay [$k_{obs(2)}$] of the 455-nm intermediate. At higher NH_2OH concentrations, $k_{obs(1)}$ was too fast to fit accurately, but, qualitatively, it increases with increasing NH_2OH concentration. The $k_{obs(2)}$ parameter showed a linear dependence on NH_2OH, consistent with a bimolecular reaction of NH_2OH and the 455-nm intermediate. A linear fit to a plot of k_{obs} versus NH_2OH concentration provided a second-order rate constant of 0.07 $mM^{-1}{\cdot}min^{-1}$ (*SI Appendix*, Fig. S8*B*).

The 455-nm intermediate was trapped for EPR characterization by freezing the reaction of 170 μM cyt P460 with 2 mM NH_2OH and 2 mM DCPIP within 1 min. The EPR spectrum of the trapped 455-nm intermediate lacks the signals associated with Fe^{III}–OH_2 and Fe^{III}–NH_2OH, suggesting that the protein is completely converted to the 455-nm intermediate or to another EPR-silent species (Fig. 4*C*). The only EPR signal observed is an $S = {}^1/_2$ signal with hyperfine structure that can be attributed to Mn^{2+} contamination in the protein sample. The lack of an Fe-based EPR signal implies that the 455-nm intermediate is either a diamagnetic or non-Kramer's (integer spin greater than 0) species.

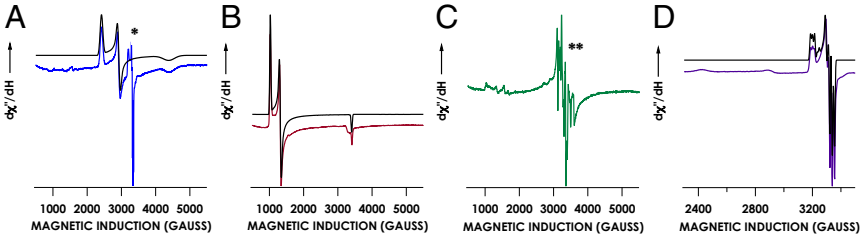

Fig. 4. EPR spectra of species on the proposed cyt P460 NH_2OH oxidase pathway. Cyt P460 at 170 μM (*A*) was treated with 100 mM NH_2OH (*B*), with 2 mM NH_2OH and 2 mM DCPIP (*C*), or with 45 mM NH_2OH and 2 mM DCPIP (*D*) and incubated for 10 min. Black traces are spectra simulated with the parameters listed in *SI Appendix*, Table ST2. Spectra were collected at 10 K and 633 μW or at 20 K and 63 μW. A 5% impurity of an $\{FeNO\}^7$ species is indicated by a single asterisk. An Mn^{2+} EPR signal is indicated by double asterisks. dχ″/dH, derivative of magnetic susceptibility vs. magnetic induction.

The decay product was prepared by treating 150 μM cyt P460 with 45 mM NH_2OH and 2 mM DCPIP, followed by incubation for 10 min at room temperature. The EPR spectrum of this sample shows signals for Fe^{III}–NH_2OH and $\{FeNO\}^7$ (Fig. 4*D*). The combined spins account for the total Fe concentration in the sample, indicating the quantitative conversion of the 455-nm intermediate to either Fe^{III}–NH_2OH (80 μM) or $\{FeNO\}^7$ (70 μM), following the depletion of oxidant.

Identification of the 455-nm Intermediate as an $\{FeNO\}^6$. The need for oxidant to form the 455-nm intermediate suggests that it is an oxidized form of Fe^{III}–NH_2OH. Bari and coworkers (34) have postulated several oxidized species in their proposed mechanism of NH_2OH oxidation by HAO, including an $\{FeNO\}^7$, an $\{FeNO\}^6$, and a ferrous-nitrous acid (Fe^{II}–ONOH) species. Other possibilities include a ferric hydroxylamine radical (Fe^{III}–$^{\bullet}NH_2OH$), which has been proposed as an intermediate in the enzymatic pathway of P450 NO reductase (35, 36) and Fe^{II}–HNO, which has been characterized in only one biological system, the myoglobin–HNO complex (37, 38). Finally, because N_2O is the product of NH_2OH oxidation by cyt P460 under our experimental conditions, an Fe–N_2O complex is also possible. We propose that our experimental data are most consistent with assignment of the 455-nm intermediate as an $\{FeNO\}^6$ species (*vide infra*).

The number of oxidizing equivalents required to convert Fe^{III}–NH_2OH to the 455-nm intermediate was determined by treating cyt P460 with substoichiometric NH_2OH and excess cyt *c* (*SI Appendix*, Fig. S9). The reduction of cyt *c* was monitored by the increase in absorption at 550 nm (ε_{550} = 19,600 $M^{-1}{\cdot}cm^{-1}$ (39). These experiments show that 3 electrons are required to oxidize Fe^{III}–NH_2OH to the 455-nm intermediate, suggesting an $\{FeNO\}^6$ or Fe^{II}–ONOH species (33). Consistent with this observation, treatment of Fe^{III}–OH_2 with NO supplied either as the gas or via the NO donor PROLI-NONOate [1-(hydroxy-NNO-azoxy)-L-proline] produces an EPR-silent species with an absorption spectrum identical to the absorption spectrum of the 455-nm intermediate (Fig. 3). The lack of an EPR signal precludes assignment of the 455-nm intermediate as an $\{FeNO\}^7$, because these species typically exhibit $S = {}^1/_2$ EPR signals (32). The 455-nm intermediate generated in this way persists for *ca.* 1 h and is stable to excess DCPIP (*SI Appendix*, Fig. S10). This lack of reactivity is inconsistent with the hypothesis of Bari and coworkers (34) that the hydrolysis of an $\{Fe–NO\}^6$ generates an Fe^{II}–ONOH adduct that is poised for proton-coupled, one-electron oxidation to NO_2^- because cyt P460 does not produce NO_2^- under anaerobic conditions. Taken together, these data support the assignment of the 455-nm intermediate as an $\{FeNO\}^6$.

The stability of the $\{FeNO\}^6$ intermediate in the absence of NH_2OH and the NH_2OH dependence of its decay suggests that $\{FeNO\}^6$ reacts with NH_2OH to form N_2O. A so-called shunted $\{FeNO\}^6$ species was prepared by adding 2 eq of NO supplied via PROLI-NONOate to cyt P460. The addition of 2 mM NH_2OH results in the decay of $\{FeNO\}^6$ to Fe^{III}–NH_2OH (*SI Appendix*, Fig. S11). Consumption of the shunted $\{FeNO\}^6$ exhibits the same NH_2OH concentration dependence, 0.07 ± .01 $mM^{-1}{\cdot}min^{-1}$, as the $\{FeNO\}^6$ that accumulates under turnover conditions.

To confirm the production of N_2O in the above reaction, cyt P460 was treated with varying concentrations of NO and excess NH_2OH. The amount to N_2O produced was monitored by GC/mass spectrometry (MS). There is a clear 1:1 stoichiometry of N_2O produced versus NO added (*SI Appendix*, Fig. S12*A*). This result is consistent with NO binding to cyt P460 to form the $\{FeNO\}^6$ intermediate and subsequent reaction with NH_2OH to form N_2O. The same experiment was performed with NO and isotopically labeled $^{15}NH_2OH$. The mass shift from 44 atomic mass units (amu) to 45 amu (*SI Appendix*, Fig. S12*B*) in the presence of cyt P460 clearly demonstrates that NO is coupled to NH_2OH via cyt P460. The reaction of NO with NH_2OH in the absence of cyt P460 does not result in N_2O production.

Mechanism for N_2O Formation from NH_2OH by Cyt P460. Given the above results, we propose the mechanism described in Fig. 5 for the NH_2OH oxidase activity of cyt P460. The catalytic cycle initiates from the $S = {}^5/_2$ Fe^{III}–OH_2, which binds NH_2OH to form an $S = {}^1/_2$ Fe^{III}–NH_2OH species that is stable in the absence of oxidant. In the presence of oxidant, Fe^{III}–NH_2OH is rapidly oxidized by 3 electrons to the EPR-silent $\{FeNO\}^6$, which undergoes nucleophilic attack by a second equivalent of NH_2OH to yield N_2O and H_2O. We propose that the Fe-containing product of this reaction is an Fe^{II} species that is rapidly oxidized and converted to the starting Fe^{III}–OH_2 species.

Several other intermediates can be envisioned in the conversion of Fe^{III}–OH_2 to $\{FeNO\}^6$. One-electron ($K_3[Fe(CN)_6]$, Cu^{II}-azurin, and $[Ru(NH_3)_6]Cl_3$) and two-electron (DCPIP and PMS) oxidants can access $\{FeNO\}^6$, which suggests that rapid, subsequent one-electron oxidation steps occur in the conversion of Fe^{III}–NH_2OH to $\{FeNO\}^6$. Although $\{FeNO\}^7$ appeared under certain conditions (i.e., after complete consumption of oxidant), it is not a catalytically competent intermediate. The EPR spectrum of this species is consistent with a five-coordinate $\{FeNO\}^7$ (32); however, a six-coordinate $\{FeNO\}^7$ could be on the reaction pathway. Other possible one-electron oxidized intermediates include Fe^{III}–$^{\bullet}NH_2OH$, Fe^{III}–$^{\bullet}NHOH$, or $\{FeN(H)O\}^{8\prime}$ (40). To date, we have found no evidence to exclude any of these possibilities, and the characterization of these possible intermediates is the subject of future investigations in our laboratory.

The rate-determining step of the anaerobic oxidation of NH_2OH by cyt P460 is the bimolecular reaction of NH_2OH with $\{FeNO\}^6$ that results in N_2O formation. The intensities of the UV/visible absorption spectral features of Fe^{III}–OH_2 treated with NO are identical to the intensities observed for the $\{FeNO\}^6$ intermediate formed using NH_2OH and oxidant (Fig. 3). Combined with the lack of Fe-based EPR signals in these samples, these data suggest that under both conditions, all Fe sites are quantitatively converted to the $\{FeNO\}^6$ species. This quantitative accumulation is consistent with the nucleophilic attack by NH_2OH being the rate-determining step of the catalytic cycle. There is precedent for NH_2OH reacting with $[Fe(CN)_5(NO)]^{2-}$, a classic example of an $\{FeNO\}^6$, to form N_2O with stoichiometry matching the stoichiometry above for cyt P460 (41).

We propose that NH_2OH reacts with $\{FeNO\}^6$ to form an Fe^{II} species, which is rapidly oxidized to return the enzyme to Fe^{III}–OH_2. This proposal is based on the precedent that $[Fe(CN)_5NO]^{2-}$ reacts with NH_2OH to form $[Fe(CN)_5(OH_2)]^{3-}$. However, the characteristic 463-nm UV/visible absorption peak of Fe^{II} cyt P460 was never observed in our experiments as an intermediate or an end product. The Fe^{II} cyt P460 is expected to react rapidly with other species present during turnover (oxidant, NH_2OH, or NO), thereby precluding its observation (*vide infra*). The reaction of Fe^{II} cyt P460 with NO produces the same inactive $\{FeNO\}^7$ species observed when Fe^{III}–OH_2 is treated with HNO (*SI Appendix*, Fig. S4). Fe^{II} cyt P460 reacts with NH_2OH to form Fe^{III}–OH_2 via an intermediate with a UV/visible absorption feature at 663 nm that has not been observed in any of our other experiments (*SI Appendix*, Fig. S13). This 663-nm intermediate forms and disappears within 3 s; assignment of this 663-nm intermediate will require rapid-mixing techniques. Critically, the reaction of Fe^{II} cyt P460 with NH_2OH does not inactivate the enzyme.

Stopped-flow UV/visible absorption spectroscopy provided insight into why inactivation of the enzyme by NO is avoided during turnover (*SI Appendix*, Fig. S14). Fe^{II} cyt P460 is quantitatively oxidized to Fe^{III}–OH_2 by $[Ru(NH_3)_6]Cl_3$ within the time of mixing

(<3 ms), placing a lower limit on k_{obs} of 1,100 s^{-1}. The reactions with NH_2OH and NO exhibit k_{obs} of 1.3 s^{-1} and 2.8 s^{-1}, respectively. These results show that oxidation of Fe^{II} cyt P460 to Fe^{III}–OH_2 is much faster than the reaction with NH_2OH or NO, thereby avoiding the production of inactive $\{FeNO\}^7$. After the oxidant is completely consumed, Fe^{II} cyt P460 will react with either NH_2OH or NO. The reaction of Fe^{II} cyt P460 with NH_2OH forms Fe^{III}–OH_2 or, in the case of high NH_2OH concentration, Fe^{III}–NH_2OH, whereas the reaction of Fe^{II} cyt P460 with NO results in the formation of inactive $\{FeNO\}^7$. Therefore, these reactions with Fe^{II} cyt P460 likely account for the products observed in the EPR spectrum of the $\{FeNO\}^6$ intermediate decay sample (Fig. 5*D*).

The King–Altman method (42) was used to derive a steady-state equation based on the minimal mechanism shown in Fig. 5. In this simplified model, NH_2OH binding is treated as reversible, with association (k_1) and dissociation (k_{-1}) rate constants. Both the Fe^{III}–NH_2OH oxidation (k_2) and the subsequent reaction of $\{FeNO\}^6$ with NH_2OH (k_3) are assumed to be irreversible. The resulting model (Eqs. **2**–**4**) indicates that k_2[ox] influences both k_{cat} and K_m:

$$\frac{velocity}{[\text{cyt P460}]_0} = \frac{k_2[\text{ox}][NH_2OH]_0}{K_m + [NH_2OH]_0}, \quad [2]$$

$$K_m = \frac{k_{-1}k_3 + k_2[\text{ox}](k_1 + k_3)}{k_1k_3}, \quad [3]$$

$$k_{cat} = k_2[\text{ox}]. \quad [4]$$

There are two limiting regimes of the derived steady-state model in which either $k_{-1}k_3$ or $k_2[\text{ox}](k_1 + k_3)$ dominates the numerator of the K_m term. In the former, K_m should resemble $K_{d(NH_2OH)}$, which was determined to be 9 mM. The steady-state activity plot lacks any clear curvature despite the inclusion of activity measurements in up to 20 mM NH_2OH. This lack of curvature suggests that the second regime, which is highly dependent on k_2[ox], contributes substantially under the assay conditions, thereby increasing the observed K_m. Currently, we have an estimate of only k_3 (0.07 $mM^{-1}{\cdot}min^{-1}$). Given the assumptions made, we attribute the absence of saturation in the steady-state activity plot to a large K_m, which suggests a large second-order rate constant for Fe^{III}–NH_2OH oxidation.

N. europaea tolerates at least 10 mM NH_2OH without showing inhibited O_2 uptake (43). Under the steady-state conditions studied, we estimate the rate of N_2O production at 10 mM NH_2OH to be 23 μM N_2O min^{-1}. The properties of the oxidant heavily influence k_2 and, by extension, the rate at which N_2O is produced by cyt P460. Thus, lacking the identity of the native electron transfer partner, we cannot verify that this rate is the physiological rate.

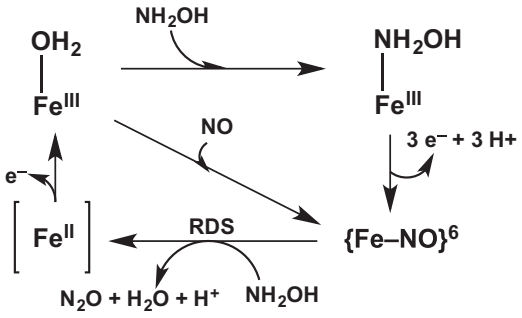

Fig. 5. Proposed Cyt P460 NH_2OH oxidase mechanism. RDS, rate-determining step.

The observation that NO binding accesses a shunt in the cyt P460 catalytic pathway provides evidence for the hypothesis that cyt P460 contributes to NO detoxification in the cell (11). Furthermore, if NO binding is reversible, there may be an alternate cyt P460 NH_2OH oxidation pathway that results in NO as the product. At low NH_2OH concentrations, the bimolecular reaction with $\{FeNO\}^6$ should be slow and NO dissociation may outpace N_2O formation. This alternate NO-forming pathway could also be responsible for the observation of NO_2^- formation under aerobic conditions, as NO reacts with O_2 in aqueous solution to form NO_2^-. To test this hypothesis, $\{FeNO\}^6$ was generated by treating Fe^{III}–OH_2 with 1 eq of NO generated from PROLI-NONOate. Exposure of the resulting $\{FeNO\}^6$ species to O_2 results in the return to Fe^{III}–OH_2 and generation of NO_2^- (*SI Appendix*, Fig. S15). We therefore propose that the NO_2^- observed as an aerobic product is not directly formed by cyt P460, but rather is a byproduct resulting from NO dissociation from the $\{FeNO\}^6$ intermediate. A detailed kinetic analysis will determine the partitioning between the NO_2^-- and N_2O-forming pathways.

Cell-free extracts of *N. europaea* were previously shown to oxidize NH_2OH to N_2O and NO without formation of NO_2^- (44). Furthermore, purified HAO was shown to react with NH_2OH and PMS or DCPIP under aerobic conditions to form a mixture of products, including NO, N_2O, NO_2^-, and NO_3^- (15). Additionally, a stable $\{FeNO\}^6$ species on the HAO P460 cofactor was observed after Fe^{III}–OH_2 was allowed to react with NO in the absence of NH_2OH (25). Given this evidence, our results, and the recent report that an HAO-like protein oxidizes NH_2OH to NO (27), we suggest that the biochemistry of HAO be revisited to determine if NO_2^- is indeed its terminal, enzymatic product.

Outlook: Environmental Consequences. AOB are major contributors to N_2O emissions from wastewater treatment plants (WWTPs), at which *N. europaea* is the dominant AOB species (45). There are two proposed methods for N_2O emission from AOB: The first is as a product in the nitrifier denitrification pathway, and the second is as a byproduct in incomplete NH_2OH oxidation. The results of our study demonstrate that the constitutively expressed cyt P460 is a direct link between NH_2OH oxidation and the emission of N_2O from *N. europaea*, thus establishing an alternative oxidative pathway to N_2O. We have established through GC and kinetic analysis a strict stoichiometry of 2 eq of NH_2OH and 4 oxidizing equivalents to produce 1 eq of N_2O. Due to the reactivity of NH_2OH with biological electrophiles, *N. europaea* likely has a detoxifying role at high NH_2OH concentrations. Previously, cyt P460 was thought to oxidize NH_2OH and NO to NO_2^- (46). However, we suggest herein an alternative role in NH_2OH detoxification through the production of N_2O (*vide supra*) (11).

We have demonstrated the production of N_2O from NH_2OH oxidation by cyt P460 under anaerobic conditions, thereby establishing a direct enzymatic link between nitrification and N_2O formation via NH_2OH. The identification of the source of N_2O emission helps to explain the production of N_2O in WWTPs under conditions of low dissolved O_2 concentrations and high NH_3 concentrations, conditions in which the nitrifier denitrification pathway would not dominate (47). The influx of high concentrations of NH_3 in WWTPs causes an increase in NH_3 oxidation rates, which, in turn, increases intracellular NH_2OH concentration (4). Studies using activated sludge from WWTPs with high concentrations of NH_3 have shown that transitioning from an aerobic environment to an anoxic environment increases the amount of N_2O released. Isotopic labeling studies show that the N_2O produced under these conditions originates from the NH_2OH oxidation pathway rather than the nitrifier denitrification pathway (48). Our study pinpoints direct N_2O production via an enzymatic, anaerobic NH_2OH oxidation mechanism. Identifying

the chemical source of this emission should aid in the design and operation of WWTPs with curtailed N_2O emission.

Experimental Procedures

Materials. Cyt P460 was prepared as previously described (29). PROLI-NONOate and $Na_2N_2O_3$ (Angeli's salt) were purchased from Cayman Chemicals. DCPIP was purchased from Alfa Aesar, PMS from Bean Town Chemical, and $NH_2OH{\cdot}HCl$ from TCI Chemicals.

Spectroscopy. X-band (9.40-GHz) EPR spectra were obtained using a Bruker Elexsys-II spectrometer equipped with a liquid He cryostat maintained at 10 or 20 K. Temperatures and microwave powers are listed in the figure legends. UV/visible absorption spectra were obtained using a Cary 60 UV/visible absorption spectrometer.

N_2O Quantification. All reactions were prepared and sealed in 5-mL headspace GC vials (Wheaton). The final N_2O concentration was analyzed with GC (Agilent), GC/MS (GC-MATE II; JEOL), or an N_2O microsensor housed within a septum-piercing needle (Unisense). For GC experiments, the headspace was measured with GC analysis using a Supel-Q PLOT (30 mm × 0.32 mm) or an RT Q-bond column. For N_2O microsensor measurement, the needle probe was inserted through the septum and into the solution. Calibration standards for all experiments were made either by diluting an N_2O-saturated solution into water or by decomposing $Na_2N_2O_3$ in Hepes buffer, pH 8.0, in a sealed headspace vial.

ACKNOWLEDGMENTS. We thank Boris Dzikovski for assistance with EPR data collection and Ivan Keresztes for assistance with GC/MS. We thank Cedric Mason for assistance with GC analysis in the Soil and Water Group's laboratory (Department of Biological and Environmental Engineering, Cornell University). We thank Samantha N. MacMillan for thoughtful discussion and a careful read of this manuscript. K.M.L. thanks the Cornell University College of Arts and Sciences for startup funding and the Department of Energy Office of Science for support in the form of an Early Career Award (DE-SC0013997). EPR data were collected at the National Biomedical Center for Advanced ESR Technology, which is supported by the National Institute of General Medical Sciences of the NIH under Award P41GM103521.

1. Ravishankara AR, Daniel JS, Portmann RW (2009) Nitrous oxide (N_2O): The dominant ozone-depleting substance emitted in the 21st century. *Science* 326(5949):123–125.
2. Goreau TJ, et al. (1980) Production of NO_2^- and N_2O by nitrifying bacteria at reduced concentrations of oxygen. *Appl Environ Microbiol* 40(3):526–532.
3. Inamori Y, Wu X-L, Mizuochi M (1997) N_2O producing capability of *Nitrosomonas europaea*, *Nitrobacter winogradskyi*, and *Alcaligenes faecalis*. *Water Sci Technol* 36(10):65–72.
4. Ni B-J, Peng L, Law Y, Guo J, Yuan Z (2014) Modeling of nitrous oxide production by autotrophic ammonia-oxidizing bacteria with multiple production pathways. *Environ Sci Technol* 48(7):3916–3924.
5. Perez-Garcia O, Villas-Boas SG, Swift S, Chandran K, Singhal N (2014) Clarifying the regulation of NO/N_2O production in *Nitrosomonas europaea* during anoxic-oxic transition via flux balance analysis of a metabolic network model. *Water Res* 60: 267–277.
6. Sabba F, Picioreanu C, Pérez J, Nerenberg R (2015) Hydroxylamine diffusion can enhance N_2O emissions in nitrifying biofilms: A modeling study. *Environ Sci Technol* 49(3):1486–1494.
7. Hooper AB, Vannelli T, Bergmann DJ, Arciero DM (1997) Enzymology of the oxidation of ammonia to nitrite by bacteria. *Antonie van Leeuwenhoek* 71(1-2):59–67.
8. Walker CB, et al. (2010) *Nitrosopumilus maritimus* genome reveals unique mechanisms for nitrification and autotrophy in globally distributed marine crenarchaea. *Proc Natl Acad Sci USA* 107(19):8818–8823.
9. Ensign SA, Hyman MR, Arp DJ (1993) In vitro activation of ammonia monooxygenase from Nitrosomonas europaea by copper. *J Bacteriol* 175(7):1971–1980.
10. Vajrala N, et al. (2013) Hydroxylamine as an intermediate in ammonia oxidation by globally abundant marine archaea. *Proc Natl Acad Sci USA* 110(3):1006–1011.
11. Stein LY (2011) Surveying N2O-producing pathways in bacteria. *Methods Enzymol* 486:131–152.
12. Stein L (2011) Heterotrophic nitrification and nitrifier denitrification. *Nitrification*, eds Ward BB, Arp DJ, Klotz MG (ASM Press, Washington, DC), pp 95–116.
13. Zhu X, Burger M, Doane TA, Horwath WR (2013) Ammonia oxidation pathways and nitrifier denitrification are significant sources of N_2O and NO under low oxygen availability. *Proc Natl Acad Sci USA* 110(16):6328–6333.
14. Smith PA, Hein GE (1960) The alleged role of nitroxyl in certain reactions of aldehydes and alkyl halides. *J Am Chem Soc* 82(21):5731–5740.
15. Hooper AB, Terry KR (1979) Hydroxylamine oxidoreductase of Nitrosomonas. Production of nitric oxide from hydroxylamine. *Biochim Biophys Acta* 571(1):12–20.
16. Beaumont HJ, van Schooten B, Lens SI, Westerhoff HV, van Spanning RJ (2004) *Nitrosomonas europaea* expresses a nitric oxide reductase during nitrification. *J Bacteriol* 186(13):4417–4421.
17. Cua LS, Stein LY (2011) Effects of nitrite on ammonia-oxidizing activity and gene regulation in three ammonia-oxidizing bacteria. *FEMS Microbiol Lett* 319(2):169–175.
18. Erickson RH, Hooper AB (1972) Preliminary characterization of a variant co-binding heme protein from Nitrosomonas. *Biochim Biophys Acta* 275(2):231–244.
19. Pearson AR, et al. (2007) The crystal structure of cytochrome P460 of *Nitrosomonas europaea* reveals a novel cytochrome fold and heme-protein cross-link. *Biochemistry* 46(28):8340–8349.
20. Bowman SE, Bren KL (2008) The chemistry and biochemistry of heme c: Functional bases for covalent attachment. *Nat Prod Rep* 25(6):1118–1130.
21. Safo MK, et al. (1992) Models of the cytochromes b. Low-spin bis-ligated (porphinato) iron (III) complexes with unusual molecular structures and NMR, EPR, and Mössbauer spectra. *J Am Chem Soc* 114(18):7066–7075.
22. Bergmann DJ, Hooper AB (1994) The primary structure of cytochrome P460 of Nitrosomonas europaea: Presence of a c-heme binding motif. *FEBS Lett* 353(3):324–326.
23. Numata M, Saito T, Yamazaki T, Fukumori Y, Yamanaka T (1990) Cytochrome P-460 of *Nitrosomonas europaea*: Further purification and further characterization. *J Biochem* 108(6):1016–1021.
24. Cabail MZ, Pacheco AA (2003) Selective one-electron reduction of *Nitrosomonas europaea* hydroxylamine oxidoreductase with nitric oxide. *Inorg Chem* 42(2):270–272.
25. Hendrich MP, Upadhyay AK, Riga J, Arciero DM, Hooper AB (2002) Spectroscopic characterization of the NO adduct of hydroxylamine oxidoreductase. *Biochemistry* 41(14):4603–4611.
26. Zahn JA, Duncan C, DiSpirito AA (1994) Oxidation of hydroxylamine by cytochrome P-460 of the obligate methylotroph *Methylococcus capsulatus* Bath. *J Bacteriol* 176(19):5879–5887.
27. Maalcke WJ, et al. (2014) Structural basis of biological NO generation by octaheme oxidoreductases. *J Biol Chem* 289(3):1228–1242.
28. Johnson KA (1992) Transient-state kinetic analysis of enzyme reaction pathways. *The Enzymes*, ed Sigman DS (Academic, Cambridge, MA), pp 1–61.
29. Elmore BO, Pearson AR, Wilmot CM, Hooper AB (2006) Expression, purification, crystallization and preliminary X-ray diffraction of a novel *Nitrosomonas europaea* cytochrome, cytochrome P460. *Acta Crystallogr Sect F Struct Biol Cryst Commun* 62(Pt 4):395–398.
30. Andersson KK, Kent TA, Lipscomb JD, Hooper AB, Münck E (1984) Mössbauer, EPR, and optical studies of the P-460 center of hydroxylamine oxidoreductase from *Nitrosomonas*. A ferrous heme with an unusually large quadrupole splitting. *J Biol Chem* 259(11):6833–6840.
31. McQuarters AB, Goodrich LE, Goodrich CM, Lehnert N (2013) Disproportionation of *O*-benzylhydroxylamine catalyzed by a ferric *bis*-picket fence porphyrin complex. *Z Anorg Allg Chem* 639(8-9):1520–1526.
32. Goodrich LE, Paulat F, Praneeth VK, Lehnert N (2010) Electronic structure of heme-nitrosyls and its significance for nitric oxide reactivity, sensing, transport, and toxicity in biological systems. *Inorg Chem* 49(14):6293–6316.
33. Enemark J, Feltham R (1974) Principles of structure, bonding, and reactivity for metal nitrosyl complexes. *Coord Chem Rev* 13(4):339–406.
34. Fernández ML, Estrin DA, Bari SE (2008) Theoretical insight into the hydroxylamine oxidoreductase mechanism. *J Inorg Biochem* 102(7):1523–1530.
35. Daiber A, et al. (2002) Isotope effects and intermediates in the reduction of NO by P450(NOR). *J Inorg Biochem* 88(3-4):343–352.
36. Lehnert N, Praneeth VK, Paulat F (2006) Electronic structure of iron(II)-porphyrin nitroxyl complexes: Molecular mechanism of fungal nitric oxide reductase (P450nor). *J Comput Chem* 27(12):1338–1351.
37. Kumar MR, Fukuto JM, Miranda KM, Farmer PJ (2010) Reactions of HNO with heme proteins: New routes to HNO-heme complexes and insight into physiological effects. *Inorg Chem* 49(14):6283–6292.
38. Lin R, Farmer PJ (2000) The HNO adduct of myoglobin: Synthesis and characterization. *J Am Chem Soc* 122(10):2393–2394.
39. Yonetani T (1965) Studies on cytochrome c peroxidase. II. Stoichiometry between enzyme, H_2O_2, and ferrocytochrome *c* and enzymic determination of extinction coefficients of cytochrome *c*. *J Biol Chem* 240(11):4509–4514.
40. McQuarters AB, Wirgau NE, Lehnert N (2014) Model complexes of key intermediates in fungal cytochrome P450 nitric oxide reductase (P450nor). *Curr Opin Chem Biol* 19: 82–89.
41. Wolfe SK, Andrade C, Swinehart J (1974) Kinetic studies of the pentacyanonitrosylferrate (2-) azide and hydroxylamine reactions. *Inorg Chem* 13(11):2567–2572.
42. King EL, Altman C (1956) A schematic method of deriving the rate laws for enzyme-catalyzed reactions. *J Phys Chem* 60(10):1375–1378.
43. Böttcher B, Koops H-P (1994) Growth of lithotrophic ammonia-oxidizing bacteria on hydroxylamine. *FEMS Microbiol Lett* 122(3):263–266.
44. Ritchie GA, Nicholas DJ (1972) Identification of the sources of nitrous oxide produced by oxidative and reductive processes in *Nitrosomonas europaea*. *Biochem J* 126(5): 1181–1191.
45. Gao J, Luo X, Wu G, Li T, Peng Y (2014) Abundance and diversity based on amoA genes of ammonia-oxidizing archaea and bacteria in ten wastewater treatment systems. *Appl Microbiol Biotechnol* 98(7):3339–3354.
46. Elmore BO, Bergmann DJ, Klotz MG, Hooper AB (2007) Cytochromes P460 and c′-beta; A new family of high-spin cytochromes *c*. *FEBS Lett* 581(5):911–916.
47. Khalil K, Mary B, Renault P (2004) Nitrous oxide production by nitrification and denitrification in soil aggregates as affected by O_2 concentration. *Soil Biol Biochem* 36(4):687–699.
48. Law Y, Ni B-J, Lant P, Yuan Z (2012) N_2O production rate of an enriched ammonia-oxidising bacteria culture exponentially correlates to its ammonia oxidation rate. *Water Res* 46(10):3409–3419.